PERGAMON

European Journal of Cancer 36 (2000) 675–681

European Journal of Cancer

www.ejconline.com

Imaging of tumour neovasculature by targeting the TGF-β binding receptor endoglin

S. Bredow *, M. Lewin, B. Hofmann †, E. Marecos, R. Weissleder

Center for Molecular Imaging Research, Massachusetts General Hospital/Harvard Medical School, Department of Radiology, 149, 13th Street, 5416, Charlestown, MA 02129, USA

Received 26 July 1999; received in revised form 27 October 1999; accepted 29 October 1999

Abstract

In vivo imaging of endothelial markers in intact tumour neovasculature would have applications in assessing the efficacy of anti-angiogenic agents in clinical trials. Although a variety of different endothelial markers have been described, few have been evaluated as imaging markers. The transforming growth factor-β (TGF-β) binding receptor endoglin is a proliferation-associated endothelial marker. We hypothesised that endoglin would be an ideal target for imaging since it is strongly upregulated in proliferating endothelial cells of the tumour neovasculature. We used a radiolabelled monoclonal anti-endoglin antibody and compared its neovascular binding, accumulation and *in vivo* behaviour to an isotype-matched control IgG_{2a}. Our data show that the probe binds specifically and rapidly within minutes *in vivo* and that correlative autoradiography and immunohistology support the *in vivo* imaging findings. Imaging of abundantly expressed endothelial targets circumvents delivery barriers normally associated with other tumour targeting strategies, and can potentially be used to quantitate molecular angiogenic markers.

Keywords: TGF-β receptor; Endoglin; Tumour neovasculature; Angiogenesis; Imaging

1. Introduction

Proliferating endothelial cells (ECs) in tumour neovasculature differ from normally quiescent endothelial cells with regard to morphology, metabolism, gene regulation, biochemical and immunological characteristics [1,2]. Targeting proliferating ECs for therapeutic purposes has been heralded as a unique strategy for controlling angiogenesis in tumours [3]. First there are minimal delivery barriers to luminally expressed surface molecules. Second, destruction of only a small number of tumour endothelial cells can potentially lead to the death of many tumour cells. Third, there is an apparent lack of drug resistance to most anti-angiogenic agents [4]. Over the past few years, several endothelial markers have been identified (reviewed in [5]) of which several have been tested for therapeutic purposes [6,7]. Non-invasive quantitation of angiogenesis ('angiogenic burden') by *in vivo* imaging of such markers at a molecular level would be invaluable in choosing appropriate therapies, determining the efficacy of anti-angiogenic therapies, and establishing appropriate lengths of treatments [8].

Several strategies of imaging tumour neovasculature have been described, amongst them methods to measure anatomical and physiological parameters (e.g. blood volume, blood flow and capillary permeability) [9,10]. More recently, specific targeting approaches such as directing fluorescently labelled antibody fragments against the fibronectin isoform B-FN [11] or antibodies conjugated to paramagnetic liposomes against $\alpha_v\beta_3$ integrins [12] have been used. The data from these *in vivo* molecular imaging approaches support the assumption that the ideal endothelial target should be one that is (1) over-expressed in proliferating but not normal endothelium and (2) located in large numbers on the luminal surface, readily available for binding of the imaging probe.

One of the markers on proliferating endothelium to potentially fulfill the requirements for diagnostic

* Corresponding author. Tel.: +1-617-726-5788/5789; fax: +1-617-726-5708.

E-mail address: bredow@helix.mgh.harvard.edu (S. Bredow).

† Current address: Institut für Diagnostikforschung GmbH, 14050 Berlin, Germany.

0959-8049/00/$ - see front matter
PII: S0959-8049(99)00335-4

imaging and cancer therapy is the transforming growth factor-β (TGF-β) binding receptor endoglin (CD 105) [13]. Prior research has shown that quiescent human endothelial cells express endoglin only weakly [14,15]. However, the expression of the receptor is strongly upregulated on the endothelium of tissues undergoing angiogenesis [16]. In contrast, the murine form of the receptor is also constitutively found on blood vessels of normal organs in this species [17]. A few studies have further confirmed the feasibility of using this TGF-β receptor as a model target for anti-angiogenic treatment [6,7].

In spite of its attractiveness as a target, no study to date has exploited the uniqueness of endoglin for imaging neovasculature. Here we demonstrate the feasibility of using endoglin as an imaging marker since low doses of a labelled anti-endoglin ^{111}In-tagged monoclonal antibody bind specifically and rapidly *in vivo*. The small amounts of probe required and the high level of expressed endoglin (up to 10^6 molecules/proliferating cell [18]) result in a theoretically ideal scenario for *in vivo* imaging.

2. Materials and methods

2.1. Cell culture and animal model

B16 cells were obtained from amelanotic B16 melanoma tissue fragments (NCI, Frederick, MD, USA) and cultured as a monolayer in 10 cm plates (Becton Dickinson, Franklin Lakes, NJ, USA) in a humidified 6% CO_2 atmosphere (Forma Scientific, Marietta, OH, USA) at 37°C. Cells were grown in Dulbecco's modified Eagle's medium (DMEM) (Cellgro Mediatech, Washington, DC, USA) supplemented with 10% fetal bovine serum (FBS) (HyClone, Logan, UT, USA) and antibiotics. Confluent cells were passaged following mild trypsinisation, and medium was replaced twice a week. The fibroblast cell line NCTC 2071 was purchased from ATCC (Manassas, VA, USA), and cultured in RPMI medium supplemented with 10% FBS and antibiotics. Passaging of the cells was identical to that of B16 cells. B16 tumours were grown in 4–6 week-old female C57BL/6 mice (Charles River Laboratories, Wilmington, MA, USA) following subcutaneous injection with approximately 3×10^6 cells/flank. Solid tumours of approximately 6–8 mm in diameter developed within 10 days.

2.2. RNA analysis by reverse transcriptase-polymerase chain reaction (RT-PCR)

Total RNA from cells or tumour tissue was analysed by RT-PCR as previously described [19], using the mouse-specific endoglin primers designed by St Jaques and colleagues [17]. Control PCRs were performed on the same samples for the housekeeping gene β-actin using commercially available primers (CLONTECH, Palo Alto, CA, USA). Reactions were cycled 28× for endoglin and 18× for β-actin at 60°C. For each sample PCR products were mixed and analysed by agarose gel electrophoresis. Gels were photographed using the Kodak DC 40 system with BioMax software (Kodak, Rochester, NY, USA).

2.3. Radiolabelling of antibodies

All antibodies (see below) were modified with diethylenetriaminepentaacidic acid (DTPA) cyclic anhydride as previously described [20]. Non-reacted DTPA was removed by dialysis at 4°C against 10 mM tetraborate pH 8.5, 150 mM NaCl (BBS) and one change of 20 mM sodium citrate pH 6.5, 150 mM NaCl (CBS). $^{111}InCl_3$ in 50 mM HCl (NEN, Boston, MA, USA) was added to the solution, and the mixture incubated for 1 h at room temperature. The labelled antibodies were purified by size exclusion on CBS pH 7 equilibrated Sephadex G-25m (Sigma, St Louis, MO, USA) spin columns.

2.4. Image acquisition and tumour analysis

Approximately 5 μg (⩽30 μCi) of labelled antibody (either endoglin-specific rat antimouse monoclonal antibody (MAb) MJ7/18 or non-specific, isotype matched control IgG_{2a} R35-95, both from PharMingen, San Diego, CA, USA) in a volume of 50 μl 0.9% NaCl (Abbott Laboratories, North Chicago, IL, USA) were injected intravenously (i.v.) via the lateral tail vein into tumour-bearing animals. At given time points (2, 15, 60 min and 6 h) animals ($n=4$ for each time point) were anaesthetised and, following the sampling of blood, prepared for scintigraphy. Images were acquired using the 15% window over the 247 keV photopeak of ^{111}In on a small-field-of-view-γ-camera equipped with a homemade 1 mm aperture pinhole collimator and a dedicated computer system (NuMac, Goffstown, NH, USA). Standard quality assurance procedures were performed prior to imaging to calibrate the system. Imaging times were adjusted to measure 100 000 counts per animal. Analysis of the regions of interest (ROI) was done to determine the target-to-background ratio followed by determination and comparison of tumour accumulation of the experimental probe. Following scintigraphy, animals were sacrificed/perfused and tissues excised and weighed. Tumours were cut in half and either processed for immunohistology and autoradiography or counted in a γ-counter (LKB Wallac, Turku, Finland). Activity was expressed as percent injected dose per gram tissue (%ID/g). Data from the counting were corrected for physical decay and compared with a standard prepared at the same time.

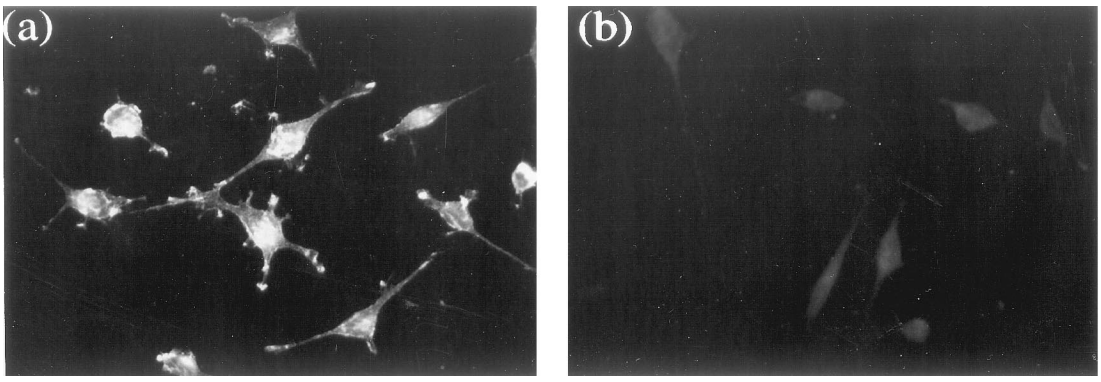

Fig. 1. Immunofluorescent detection of endoglin on the cellular membrane of NCTC 2071 fibroblasts. Cells were incubated with specific (a, 1:600 in PBS/1%BSA) or non-specific (b, same dilution) antibody followed by FITC-labelled secondary antibody (1:300 in PBS/2% goat serum). Magnification: ×400.

2.5. Immunofluorescence, immunohistochemistry and autoradiography

Sections of 8 μm thickness were cut from radioactive and non-radioactive tumours. For immunofluorescent analyses, non-radioactive sections were fixed in acetone, and cells, which were grown on coverslips, were fixed in a 1:1 mixture of acetone and methanol (all chemicals and solvents were from Sigma, St Louis, MO, USA). The samples were washed in phosphate buffered saline (PBS; Boehringer Mannheim, Indianapolis, IN, USA) and then incubated with either diluted MJ7/18 or R35-95 antibody followed by a subsequent incubation with a secondary FITC-labelled goat antirat antibody (PharMingen, San Diego, CA, USA). Analysis of the sections was done using an inverted microscope (Zeiss Axiovert 100TV, Wetzlar, Germany) fitted with a fluorescent filter set (Omega Optical, Brattleboro, VT, USA). Radioactive tumour sections were analysed by immunohistochemistry or autoradiography. For immunohistochemistry, PBS was substituted by HEPES buffered saline pH 7.5 (HBS) and the FITC-labelled secondary antibody substituted with a goat antirat antibody conjugated to alkaline phosphatase (PharMingen, San Diego, CA, USA). Prior to fixation, the sections were first incubated with the secondary antibody. Following a heat step (65°C, 30 min), phosphatase activity was visualised using nitrobluetetrazolium/chloro-indoyl phosphate (NBT/BCIP) substrate (Boehringer Mannheim, Indianapolis, IN, USA). Sections were then counterstained in nuclear fast red, dehydrated, cleared in xylene, and mounted in Permount (Fisher Scientific, Fair Lawn, NJ, USA). For autoradiography, sections were either directly exposed overnight on a PhosphorImager (Molecular Dynamics, Sunnyvale, CA, USA) followed by analysis using ImageQuant software, or dipped in Kodak nuclear track emulsion NTB2 and stored in the dark at 4°C for 2 weeks. Slides were then developed in Kodak D-19 solution, washed, and counterstained in haematoxylin.

3. Results

To target endoglin on tumour endothelium *in vivo*, we used the rat antimouse MAb MJ7/18 [21]. Specific staining of the cell membranes of the endoglin rich fibroblast cell line NCTC 2071 [17] indicated that this antibody binds to the extracellular domain of CD 105 (Fig. 1, panel a). No staining could be observed when an

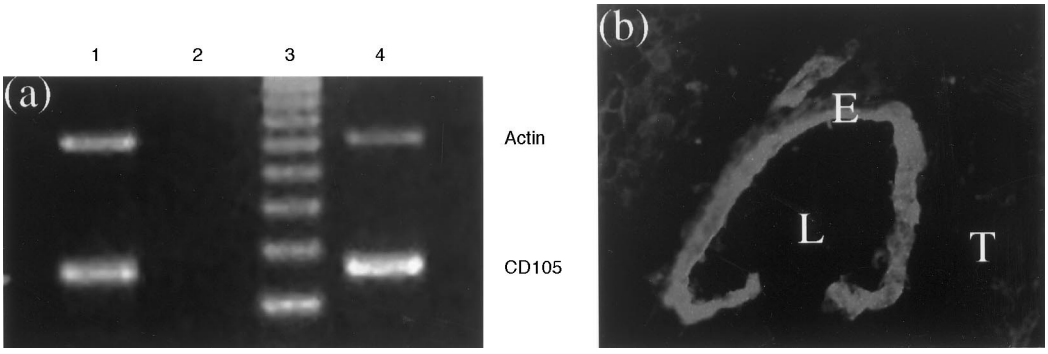

Fig. 2. Analysis of endoglin expression on endothelium of solid B16 tumours by RT-PCR (a) and immunofluorescence (b) a: lane 1: total RNA from NCTC 2071 cells; 2: H_2O control; 3: Marker-DNA (123 bp-ladder, LifeTechnologies, Gaithersburg, MD, USA); 4: total RNA from B16 tumour. b: Frozen tumour sections were treated as described in the legend for Fig. 1. E: endothelium; L: lumen; T: tumour tissue. Magnification: ×400.

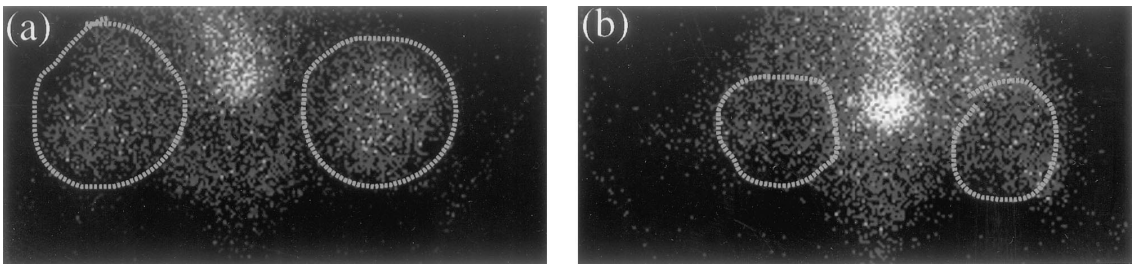

Fig. 3. Scintigraphy of B16 tumours in living animals 15 min after i.v. injection of radiolabelled MAbs. The positions of the bilateral thigh tumours are outlined. The left image (a) represents the endoglin image, whereas the right image (b) is a 'blood pool' image.

isotype-matched control antibody, R35-95, was used (Fig. 1, panel b) or when the primary antibody was omitted during the staining process.

Endoglin mRNA and protein expression in amelanotic murine B16 tumours was determined to confirm the tumour as a suitable *in vivo* model by showing that sufficient target would be present on tumour endothelium for imaging (Fig. 2). Endoglin expression appears to be regulated in part at the transcriptional level [17,22–24], and specific mRNA amounts in tumour-extracted RNAs were first measured by RT-PCR (Fig. 2, panel a, lane 4, lower band); RNAs from NCTC 2071 cells (Fig. 2, lane 1 lower band) served as positive controls, and the housekeeping gene β-actin [Fig. 2, lanes 1 and 4, upper bands of 838 base pairs (bp) respectively] was used as an endogenous control to allow for comparison of endoglin cDNAs between tumours and the NCTC 2071 cell line. The data show that the amplified cDNA fragments had the expected size (428 bp) and were detected in similar amounts.

Like other melanoma cell lines, B16 cells themselves express endoglin [25] (data not shown), and RT-PCR can, therefore, not directly differentiate between the amounts of endoglin synthesised by either tumour or mouse endothelial cells. However, analysis of protein expression by immunofluorescent staining of frozen tumor sections (Fig. 2, panel b) showed that only the luminal sides of vessels were stained distinctly above the surrounding tissue background and that the contribution from B16-expressed endoglin was weak. No endothelial staining was observed in parallel sections when either the primary MAb was omitted or when the control antibody, R35-95, was used instead.

Following i.v. injection, radiolabelled antibody accumulated in tumours of living mice (Fig. 3). The tumours in animals which had received labelled MJ7/18 were more easily identified (Fig. 3, panel a) compared with control animals which had received the control, R35-95 (Fig. 3, panel b). There was a higher background in non-tumour tissue in the control animals due to greater blood pool activity of the non-specific MAb. In these animals, for example, the aorta was always clearly visible at all time points investigated.

The two antibodies also displayed considerably different blood clearances (Table 1). Approximately 97% injected dose (ID)/g blood of MJ7/18 was removed from circulation within 15 min after administration, whilst 30% ID/g blood of labelled R35-95 remained in circulation at the same time point. At 6 h, approximately 16% ID/g blood of R35-95 could still be found in the blood pool. Using a single exponential decay model, the blood half-lives of the labelled antibodies were estimated to be <1 min for MJ7/18 and approximately 40 min for R35-95. In mice, endoglin-specific antibodies also bind to vascular endothelial cells in such tissues as liver, kidney and heart [17] (Table 1). This species shows an apparent constitutively higher expression of the receptor in such tissues in comparison to normal human organs [5,26], and staining of blood vessels with MJ7/18 can be as intense as in tumours (data not shown).

Binding of radiolabelled MJ7/18 to tumour vasculature occurred rapidly (Table 1), as there was no major

Table 1
Monoclonal antibody accumulation (expressed as % injected dose per gram tissue ± standard deviation) in various perfused murine tissues

	Time after injection							
	2 min		15 min		60 min		360 min	
Tissue	MJ7/18	R35-95	MJ7/18	R35-95	MJ7/18	R35-95	MJ7/18	R35-95
Blood	2.45 ± 1.3	55.66 ± 50.2	3.04 ± 0.4	30.36 ± 3.0	2.39 ± 0.1	17.66 ± 2.5	1.96 ± 0.1	15.66 ± 4.7
Tumour	0.75 ± 0.9	0.32 ± 0.5	1.69 ± 0.5	0.81 ± 0.8	1.67 ± 0.3	1.62 ± 0.5	1.67 ± 0.7	1.70 ± 1.4
Heart	3.17 ± 2.7	1.45 ± 1.5	6.70 ± 0.6	2.17 ± 0.9	5.08 ± 1.2	2.38 ± 0.8	4.27 ± 1.3	1.20 ± 0.9
Kidney	0.30 ± 0.2	0.31 ± 0.2	7.07 ± 6.9	3.24 ± 3.2	6.48 ± 3.8	6.03 ± 1.9	6.56 ± 6.6	1.28 ± 0.7
Liver	1.93 ± 2.4	0.12 ± 0.1	19.39 ± 15.7	2.86 ± 2.4	16.70 ± 2.6	1.40 ± 1.2	14.82 ± 9.5	1.55 ± 1.5
Lung	2.54 ± 2.6	0.04 ± 0.04	ND	2.01 ± 1.6	ND	1.40 ± 1.4	7.30 ± 5.3	3.47 ± 2.9

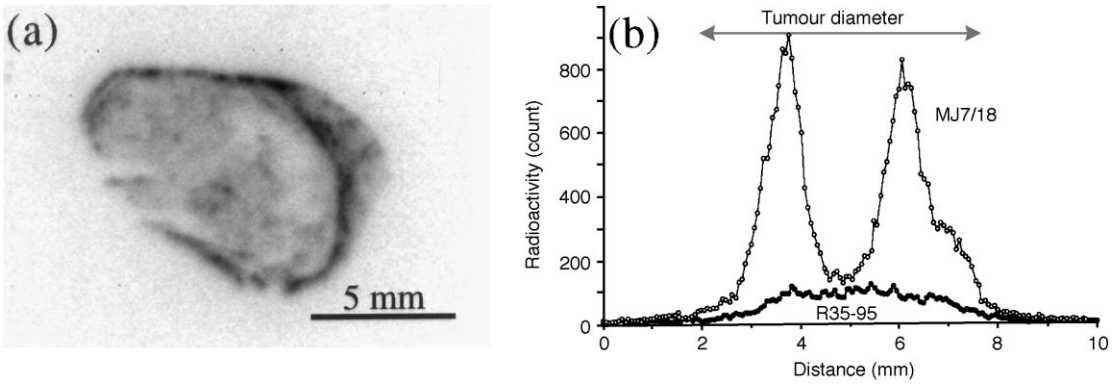

Fig. 4. Autoradiography (a) of a frozen B16 tumour section (8 μm) obtained from a tumour 45 min. after MJ7/18 injection. Comparative cross-sectional density profiles (b) of autoradiographs for tumour sections of similar size 45 min after injection with MJ7/18 (white) or R35-95 (black).

difference in accumulation at earlier (1.69 ± 0.5% ID/g tumour at 15 min) or later time points (1.67 ± 0.7% ID/g tumour at 6 h). In agreement with these data, there was no difference in the morphological appearance of tumour images, obtained in living animals over a period of 3 days (data not shown). In contrast, the non-specific antibody, R35-95, accumulated initially at a lower rate in tumours (Table 1), and slow extravasation across leaky neovasculature occurred with time as described for many antitumour antibodies [20].

Additional autoradiography and immunohistology experiments performed on individual tumours corroborated the different patterns of tumoral accumulation for the two antibodies. MJ7/18 showed intense activity in the tumour periphery (Fig. 4, panel a) where the highest concentration of vessels could be found (see below), and lower activity in the centre of all sections investigated. The tumour centres demonstrated a markedly heterogeneous distribution which varied from tumour to tumour. In contrast, little accumulation of activity could be observed either directly or by cross-sectional profile density analysis of tumour sections (Fig. 4, panel b) in identically prepared tissue sections from tumours of animals that had been injected with radiolabelled R35-95.

Histological analysis at higher resolution further confirmed that specific activity was maximally detected on the endothelium of tumour vessels in the periphery of the sections (Fig. 5, panel a). Since this activity could be demonstrated on non-fixed sections of tumours injected with MJ7/18 using the secondary antibody directly, the labelling performed on MJ7/18 did not lead to a loss of its binding ability. Analysis at higher resolution of parallel sections (Fig. 5, panel b) further confirmed that these signals were caused by intact ^{111}In-MAb complexes, targeted to the tumour endothelium of these highly vascular melanomas. Consistent with vascular binding, activity is clearly demonstrated at the endothelial surface, whilst less activity is present in tumour cells or in the extracellular space.

4. Discussion

Over 20 anti-angiogenic agents are currently in clinical trials [27]. However, there is a general lack of direct,

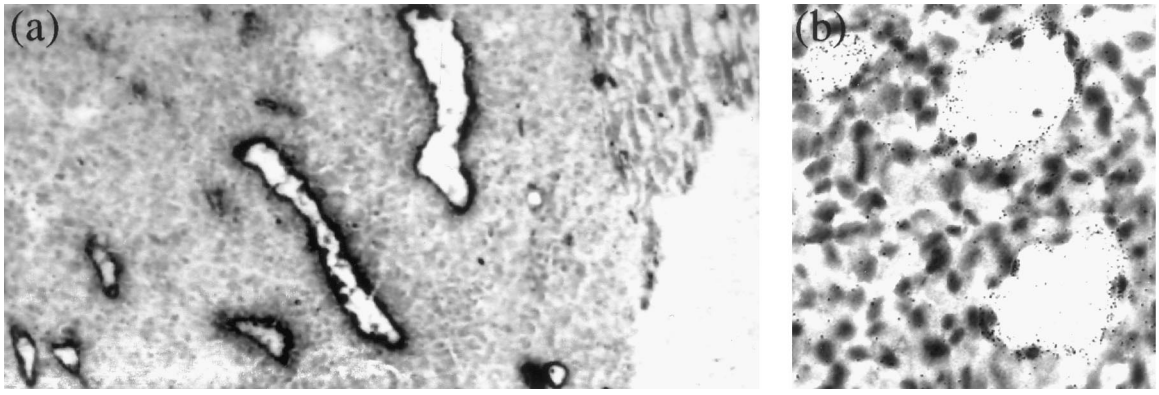

Fig. 5. Immunohistology (a) and microautoradiography (b) of B16 tumour sections obtained as described in legend for Fig. 4(a). Sections were directly incubated with secondary antibody (1:1000 in HBS/2% goat serum), magnification: ×160. (b) Black granules are mostly associated with the surface of three tumour vessels, magnification: ×640.

non-invasive methods to quantitate and measure the 'angiogenic burden' at a molecular level. Such methods would obviously be valuable in estimating treatment efficacy. Imaging of endothelial, proliferation-associated markers of tumour neovasculature potentially represents a tool to achieve this goal, but only a few studies describing this objective have been published [11,12]. In the present paper we demonstrate the feasibility of using the endothelial marker, the TGF-β binding receptor endoglin (CD 105) as a target for relatively rapid *in vivo* imaging.

Though currently no information is available about its regulation or substrates, genetic studies have shed some light on the importance of endoglin for the vasculature [28,29]. The homodimeric 180 kDa, type I integral membrane protein is a regulatory component of the TGF-β receptor complex that binds TGF-β1 and β3 with high affinity [13]. Mutations in the coding region of the gene, leading to truncated versions of the receptor cause hereditary haemorrhagic telangiectasia type 1 (HHT) [28]. Furthermore, mice devoid of endoglin die from defective vascular development by gestational day 11.5 [29].

For imaging applications, this TGF-β receptor represents an ideal target. Its expression is proliferation-associated and, in humans, is only weakly detectable on the endothelium in normal tissues [15]. In newly forming blood vessels, however, receptor densities of up to 10^6 molecules per proliferating cell have been reported [16]. In contrast, analyses of murine models, such as the one employed here, have shown that endoglin expression is not only limited to proliferating endothelium in this species, but is also found in the vasculature of normal organs [17] which explains the biodistribution findings in Table 1.

The data presented in the current study confirm the feasibility of using endoglin to image angiogenesis *in vivo*. Compared with an isotype matched MAb, the specific anti-endoglin antibody, MJ7/18, showed significant differences in biological behaviour and target binding. The stable antibody complex was quickly cleared from circulation (Table 1) due largely to binding to its specific endothelial target endoglin (Fig. 5). Image acquisition was, therefore, possible directly after injection (Fig. 3). In contrast, the control IgG, R35-95, remained mostly in circulation. The resulting 'blood pool' images and accumulation data (Table 1) were also caused by slow, nonspecific extravasation into tumour interstitium across leaky neovasculature. No 'binding' of R35-95 could be detected, but similar patterns of 'accumulation' have also been observed for other long circulating macromolecules [20].

Antibody staining was strongly pronounced in the periphery of the tumours (Fig. 4, panel a) which is the part with the highest vessel density (Fig. 5, panel a). In 8 μm sections, staining was mostly detected on the surface of neovessels with little or no staining of tumour cells (Fig. 5, panel b). Stains could also be observed in the centre of tumours. Tumours at this stage of growth showed little necrosis in this area, however, the number of vessels was considerably lower compared with the tumour rim.

Imaging endothelial targets *in vivo* is a challenging task, and it remains to be seen how many markers [5] can actually be used for imaging as the affinity probes (amongst them antibodies, peptides and aptamers) can reside in any of the following compartments during the time of imaging: (1) the circulating blood pool; (2) bound to the endothelial target; or (3) extravasated into adjacent tumour interstitium. To optimise imaging of the endothelial binding event, blood pool activity and extravasation must, therefore, be minimised. In case of the anti-endoglin imaging this was achieved by: (1) administering sufficiently small amounts of affinity ligand so as not to saturate the receptor; and (2) performing imaging shortly after injection. Although the *in vivo* images shown in Fig. 3 allow one to 'visualize' tumours with either antibody, the images represent different physiological information. Whilst the MJ7/18 image reflects anti-endoglin binding, the R35-95 image is a 'blood pool' image of the tumour.

In the current study we used planar scintigraphy to visualise *in vivo* targeting of the antibody. The observed image in Fig. 3 thus, reflects a composite of events occurring through the thickness of the entire animal. Nuclear imaging techniques have an inherently lower spatial resolution compared with spatially encoded imaging techniques like magnetic-resonance imaging. The high sensitivity, however, allows imaging of the distribution of nanomolar amounts of tracers. Alternative imaging strategies, particularly in a clinical setting, would also utilise tomographic image acquisition such as single photon emission computed tomography (SPECT) or positron emission tomography (PET) imaging.

In summary, our results indicate the feasibility of imaging endothelial targets directly *in vivo*. However, to further improve image acquisition and quantitation, alternative MAbs or a combination thereof ('cocktail') that show better specificity for 'activated' endothelium [30] also need to be evaluated. Additionally, other approaches such as clearing of blood pool activity with secondary antibodies or avidin/streptavidin strategies could be employed to avoid slower binding or higher blood pool activity of the specific probes. In the meantime, alternative methods to image physiological parameters (e.g. functional perfusion, blood volume) can also be used to quantitate the 'angiogenic burden' [9,10].

Acknowledgements

The authors would like to thank Dr U. Mahmood for critical review of the manuscript. This work was

supported by a grant from the National Institutes of Health (2-RO1 CA 59649-05). M. Lewin was supported by a grant from the French government 'Bourse Lavoisier' and the French Society of Radiology (SFR).

References

1. Folkman J. Angiogenesis in cancer, vascular, rheumatoid and other disease. *Nature Med* 1995, **1**, 27–31.
2. Shima DT, Saunders KB, Gougos A, D'Amore PA. Alterations in gene expression associated with changes in the state of endothelial differentiation. *Differentiation* 1995, **58**, 217–226.
3. Burrows FJ, Watanabe Y, Thorpe PE. A murine model for antibody-directed targeting of vascular endothelial cells in solid tumors. *Cancer Res* 1992, **52**, 5954–5962.
4. Denekamp J. Vasculature as a target for tumor therapy. *Prog Appl Microcirc* 1984, **4**, 28–38.
5. Thorpe PE, Derbyshire EJ. Targeting the vasculature of solid tumors. *J Controlled Release* 1997, **48**, 277–288.
6. Burrows F, Derbyshire E, Tazzari P, *et al*. Up-regulation of endoglin on vascular endothelial cells in human solid tumors: implications for diagnosis and therapy. *Clin Cancer Res* 1995, **1**, 1623–1634.
7. Matsuno F, Haruta Y, Kondo M, Tsai H, Barcos M, Seon BK. Induction of lasting complete regression of preformed distinct solid tumors by targeting the tumor vasculature using two new anti-endoglin monoclonal antibodies. *Clin Cancer Res* 1999, **5**, 371–382.
8. Passe TJ, Bluemke DA, Siegelman SS. Tumor angiogenesis: tutorial on implications for imaging. *Radiology* 1997, **203**, 593–600.
9. Lewin M, Bredow S, Sergeyev N, Marecos E, Bogdanov Jr A, Weissleder R. *In vivo* assessment of VEGF induced angiogenesis. *Int J Cancer* 1999, **83**, 798–802.
10. Weissleder R, Cheng H, Marecos E, Kwong K, Bogdanov A. Mapping of tumour vascular and interstitial volume fractions non-invasively *in vivo*. *Eur J Cancer* 1998, **34**, 1448–1454.
11. Neri D, Carnemolla B, Nissim A, *et al*. Targeting by affinity-matured recombinant antibody fragments of an angiogenesis associated fibronectin isoform. *Nat Biotechnol* 1997, **15**, 1271–1275.
12. Sipkins DA, Cheresh DA, Kazemi MR, Nevin LM, Bednarski MD, Li KCP. Detection of tumor angiogenesis *in vivo* by $\alpha_v\beta_3$-targeted magnetic resonance imaging. *Nature Med* 1998, **4**, 623–626.
13. Kumar P, Wang JM, Bernabeu C. CD 105 and angiogenesis. *J Pathol* 1996, **178**, 363–366.
14. Krupinski J, Kaluza J, Kumar P, Kumar S, Wang JM. Role of angiogenesis in patients with cerebral ischemic stroke. *Stroke* 1994, **25**, 1794–1798.
15. Westphal JR, Willems HW, Schalkwijk CJM, Ruiter DJ, de Waal MW. A new 180 kDa dermal endothelial cell activation antigen: *in vitro* and *in situ* characteristics. *J Invest Dermatol* 1993, **100**, 27–34.
16. Wang JM, Kumar S, Pye D, Haboubi N, Al-Nakib L. Breast carcinoma: comparative study of tumor vasculature using two endothelial markers. *J Natl Cancer Inst* 1994, **86**, 386–388.
17. St Jaques S, Cymerman U, Pece N, Letarte M. Molecular characterization and *in situ* localization of murine endoglin reveal that it is a transforming growth factor-beta binding protein of endothelial and stromal cells. *Endocrinology* 1994, **314**, 2645–2657.
18. Cheifetz S, Bellón T, Calés C, *et al*. Endoglin is a component of the transforming growth factor β receptor system in human endothelial cells. *J Biol Chem* 1992, **267**, 19027–19030.
19. Bredow S, Guha-Thakurta N, Taishi P, Obál Jr F, Krueger JM. Diurnal variations of tumor necrosis factor alpha mRNA and alpha-tubulin mRNA in rat brain. *Neuroimmunomodulation* 1997, **4**, 84–90.
20. Marecos E, Weissleder R, Bogdanov Jr A. Antibody-mediated versus nontargeted delivery in a human small cell lung carcinoma model. *Bioconjugate Chem* 1998, **9**, 184–191.
21. Ge AZ, Butcher EC. Cloning and expression of a cDNA encoding mouse endoglin, an endothelial cell TGF-beta ligand. *Gene* 1994, **138**, 201–206.
22. Lastres P, Letamendía A, Zhang H, *et al*. Endoglin modulates cellular responses to TGF-β1. *J Cell Biol* 1996, **133**, 1109–1121.
23. Adam PJ, Clesham GJ, Weissberg PL. Expression of endoglin mRNA and protein in human vascular smooth muscle cells. *Biochem Biophys Res Commun* 1998, **247**, 33–37.
24. Letamendía A, Lastres P, Almendro N, *et al*. Endoglin, a component of the TGF-beta receptor system, is a differentiation marker of human choriocarcinoma cells. *Int J Cancer* 1998, **76**, 541–546.
25. Altomonte M, Montagner R, Fonsatti E, *et al*. Expression and structural features of endoglin (CD 105), a transforming growth factor beta1 and beta3 binding protein, in human melanoma. *Br J Cancer* 1996, **74**, 1586–1591.
26. Bodey B, Bodey Jr B, Siegel SE, *et al*. Immunocytochemical detection of endoglin is indicative of angiogenesis in malignant melanoma. *Anticancer Res* 1998, **18**, 2701–2710.
27. Harris A. Anti-angiogenesis therapy and strategies for integrating it with adjuvant therapy. *Recent Results Cancer Res* 1998, **152**, 341–352.
28. McAllister KA, Grogg KM, Johnson DW, *et al*. Endoglin, a TGF-beta binding protein of endothelial cells, is the gene for hereditary haemorrhagic telangiectasia type 1. *Nature Genet* 1994, **8**, 345–351.
29. Li DY, Sorensen LK, Brooke BS, *et al*. Defective angiogenesis in mice lacking endoglin. *Science* 1999, **284**, 1534–1537.
30. Kumar S, Ghellal A, Li C, *et al*. Breast carcinoma: vascular density determined using CD 105 antibody correlates with tumor prognosis. *Cancer Res* 1999, **59**, 856–861.